SUPPLEMENTARY INFORMATION

Title: Bi-directional processing of pri-miRNAs with branched terminal loops by Arabidopsis Dicer-like1

Hongliang Zhu[1,2,3], Yuyi Zhou[1,2,4], Claudia Castillo-González[1,2], Amber Lu[1,2], Chunxiao Ge[2,5], Ying-Tao Zhao[6], Liusheng Duan[4], Zhaohu Li[4], Michael J. Axtell[7], Xiu-Jie Wang[6], and Xiuren Zhang[1,2,5*]

[1]Department of Biochemistry and Biophysics

Texas A&M University, College Station, TX 77843, USA

[2]Institute of Plant Genomics and Biotechnology

Texas A&M University, College Station, TX 77843, USA

[3]College of Food Science and Nutritional Engineering, China Agricultural University, Beijing, 100083, China

[4]College of Agriculture and Life Science, China Agricultural University, Beijing, 100094, China

[5]Program of Molecular and Environmental Plant Sciences

Texas A&M University, College Station, TX 77843, USA

[6]State Key Laboratory of Plant Genomics, Institute of Genetics and Developmental Biology, Chinese Academy of Sciences, Datun Road, Chaoyang District, Beijing, 10101, China

[7]Department of Biology and Huck Institutes of the Life Sciences, Penn State University, University Park, PA 16802, USA

[*]Correspondence: xiuren.zhang@tamu.edu

SUPPLEMENTARY FIGURES

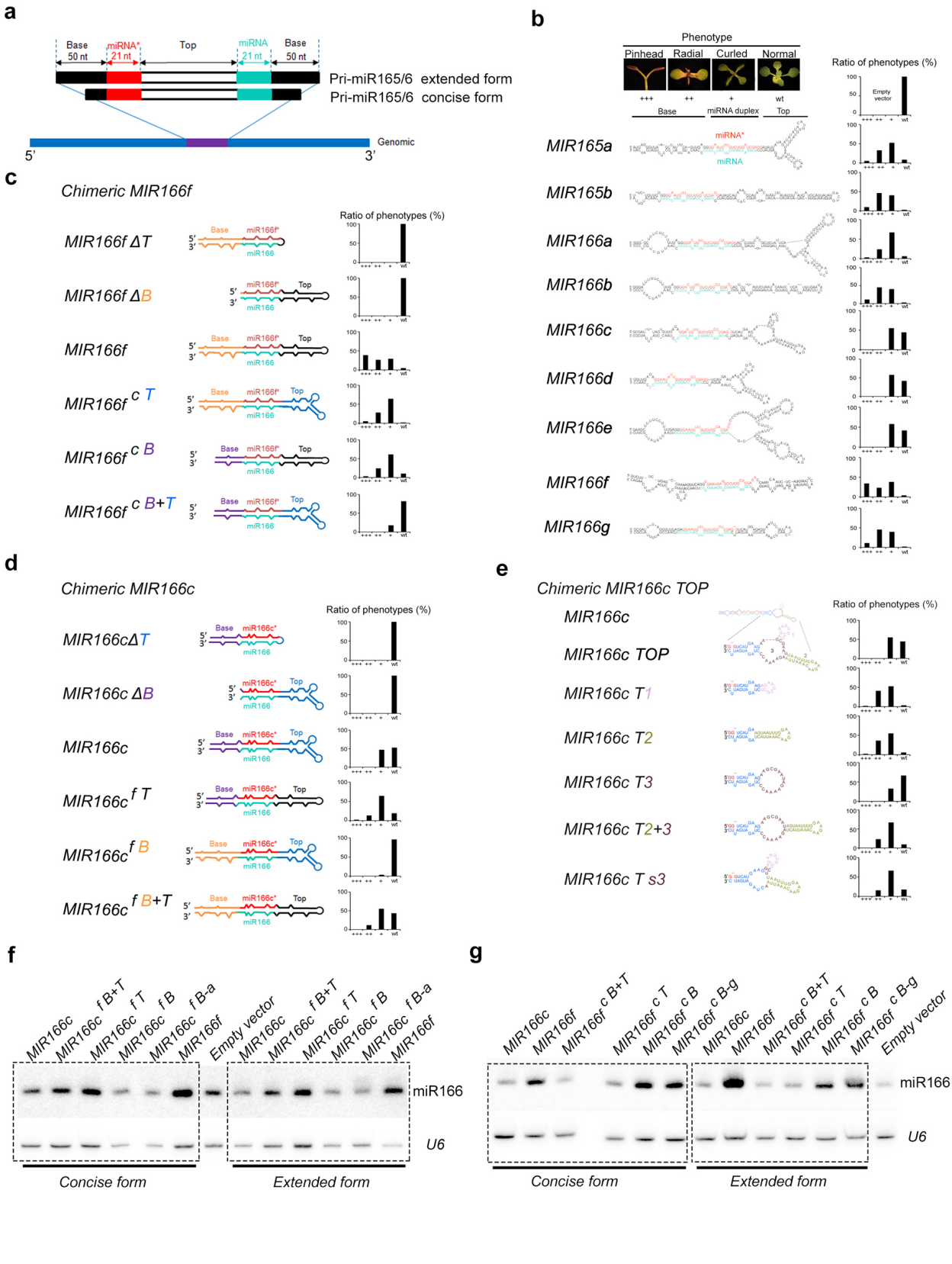
a
Base 50 nt
miRNA* 21 nt
Top
miRNA 21 nt
Base 50 nt
Pri-miR165/6 extended form
Pri-miR165/6 concise form
Genomic
5'
3'
b
Phenotype
Pinhead
Radial
Curled
Normal
+++
++
+
wt
Base
miRNA duplex
Top
Ratio of phenotypes (%)
Empty vector
miRNA*
miRNA
MIR165a
MIR165b
MIR166a
MIR166b
MIR166c
MIR166d
MIR166e
MIR166f
MIR166g
c
Chimeric MIR166f
MIR166f ΔT
MIR166f ΔB
MIR166f
MIR166f c T
MIR166f c B
MIR166f c B+T
Base
miR166f*
Top
miR166
Ratio of phenotypes (%)
d
Chimeric MIR166c
MIR166cΔT
MIR166c ΔB
MIR166c
MIR166c f T
MIR166c f B
MIR166c f B+T
Base
miR166c*
Top
miR166
Ratio of phenotypes (%)
e
Chimeric MIR166c TOP
MIR166c
MIR166c TOP
MIR166c T1
MIR166c T2
MIR166c T3
MIR166c T2+3
MIR166c T s3
Ratio of phenotypes (%)
f
MIR166c
MIR166c f B+T
MIR166c f T
MIR166c f B
MIR166c f B-a
MIR166f
Empty vector
miR166
U6
Concise form
Extended form
g
MIR166c
MIR166f
MIR166f c B+T
MIR166f c T
MIR166f c B
MIR166f c B-g
Empty vector
miR166
U6
Concise form
Extended form

Supplementary Figure 1. Transgenic plants expressing pri-miRNAs with different secondary structures displayed contrasted phenotypes and miRNA abundance. (a) Illustration of extended (~50bp lower stem) and concise (~25bp lower stem) pri-miR165-166s. (b) Phenotypic distribution for *35S-MIR165-166* T1 transformants (n>200 for each construct). Four categories of phenotypic severity are shown on top. Predicted secondary structures of concise pri-miR165-166s are displayed on left. miRNA and miRNA* are marked as turquoise and red, respectively. (c) Phenotypic distribution of T1 transgenic plants expressing *35S-MIR166f* mutants (n>200 for each construct). Schematic structures of pri-miR166f deletion mutants or chimeric mutants harboring counterparts from pri-miR166c are shown on left. (d) Phenotypic distribution of T1 transgenic plants expressing *35S-MIR166c* mutants (n>200 for each construct). Schematic structures of pri-miR166c deletion mutants or swapped mutants harboring counterparts from pri-miR166f are shown on left. (e) Phenotypic distribution of T1 transgenic plants expressing the *35S-MIR166c* mutants with various deletions in the terminal loop (n>200 for each construct). Schematic structures of the pri-miR166c terminal-loop deletion mutants are shown on left. Loops # 1, 2, and 3 are shown in pink, green yellow and purple, respectively. (f) sRNA blot analysis of miR166 processed from the concise and extended forms of pri-miR166c and chimeric pri-miR166c containing counterparts from pri-miR166f in *N. Bentha*. (g) sRNA blot analysis of miR166 processed from the concise and extended forms of pri-miR166f and chimeric pri-miR166f containing counterparts from pri-miR166c in *N. Bentha*. RNA blot was probed using 5′ end ^{32}P-labeled oligo probes complementary to miR166. *U6* serves as a loading control.

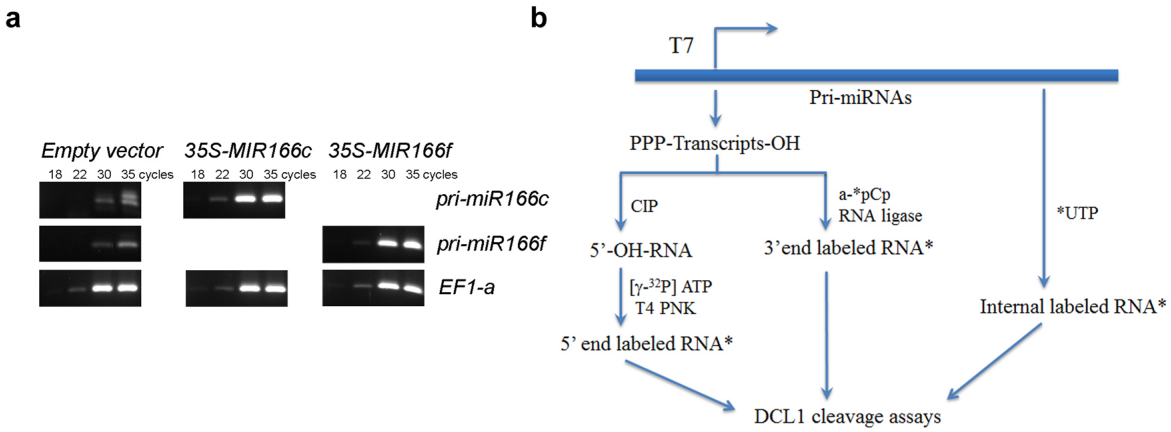
a
Empty vector
35S-MIR166c
35S-MIR166f
18 22 30 35 cycles
pri-miR166c
pri-miR166f
EF1-a
b
T7
Pri-miRNAs
PPP-Transcripts-OH
CIP
a-*pCp
RNA ligase
*UTP
5'-OH-RNA
3'end labeled RNA*
[γ-32P] ATP
T4 PNK
5' end labeled RNA*
Internal labeled RNA*
DCL1 cleavage assays

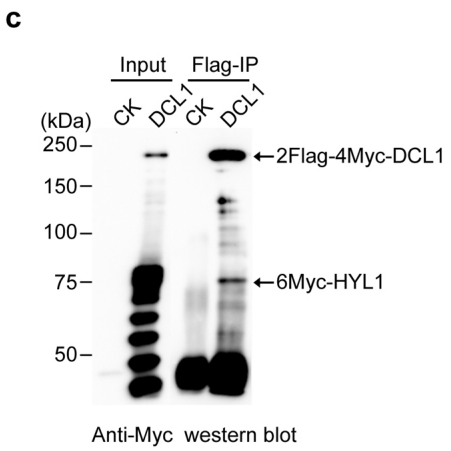
c
Input
Flag-IP
CK
DCL1
(kDa)
250
150
100
75
50
2Flag-4Myc-DCL1
6Myc-HYL1
Anti-Myc western blot

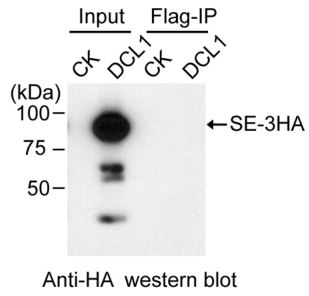
d
Input
Flag-IP
CK
DCL1
(kDa)
100
75
50
SE-3HA
Anti-HA western blot

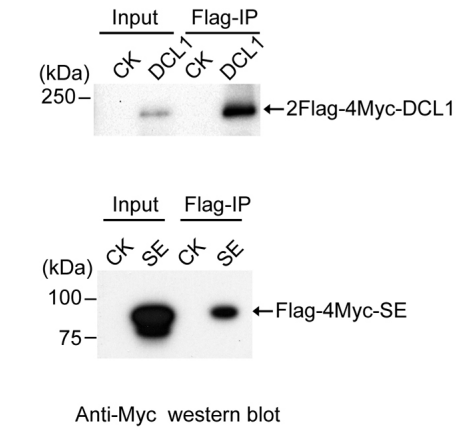
e
Input
Flag-IP
CK
DCL1
(kDa)
250
2Flag-4Myc-DCL1
SE
100
75
Flag-4Myc-SE
Anti-Myc western blot

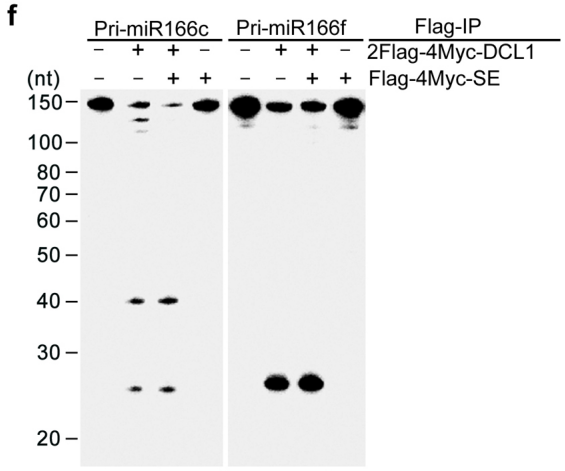
f
Pri-miR166c
Pri-miR166f
Flag-IP
2Flag-4Myc-DCL1
Flag-4Myc-SE
(nt)
150
100
80
70
60
50
40
30
20

Supplementary Figure 2. An *in vitro* DCL1 reconstitution assay system in plants. (a) Semi-RT-PCR of pri-miR166c and pri-miR166f transcripts in the pooled T1 transformants expressing *35S-MIR166c* and *35S-MIR166f*. Four PCR cycles were used for estimation of levels of pri-miRNA transcripts. *EF1-a* was an internal control. (b) Strategies for the 5′ end, 3′ end and internal labeling of RNAs. (c) Western blot analysis of DCL1–HYL1 complexes prepared from *N. Bentha*. Immunoprecipitation of DCL1 complexes was performed through two-step purification using anti-Flag and then anti-Myc antibodies. The DCL1 and HYL1 proteins (shown by arrows) were detected using a polyclonal anti-Myc antibody. (d) Western blot analysis of SE protein in the DCL1–HLY1 complexes using a monoclonal anti-HA antibody. (e) Western blot analysis of immunoprecipitates of DCL1–HYL1 complexes and single SE protein prepared through two-step purification using anti-Flag and then anti-Myc antibodies. (f) *In vitro* reconstitution of DCL1 assays with 5′ end labeled pri-miR166c and pri-miR166f with addition of SE protein prepared from immunoprecipitation. RNAs recovered from the reaction mix were fractionated on 15% denaturing gels. The positions of intact substrates, cleavage products, and RNA markers are shown.

a

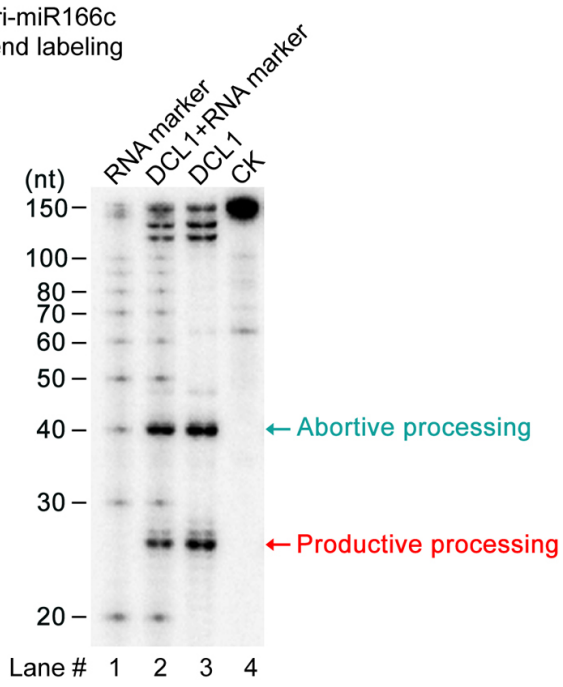
Pri-miR166c
5' end labeling
RNA marker
DCL1+RNA marker
DCL1
CK
(nt)
150
100
80
70
60
50
40
30
20
← Abortive processing
← Productive processing
Lane # 1 2 3 4

b

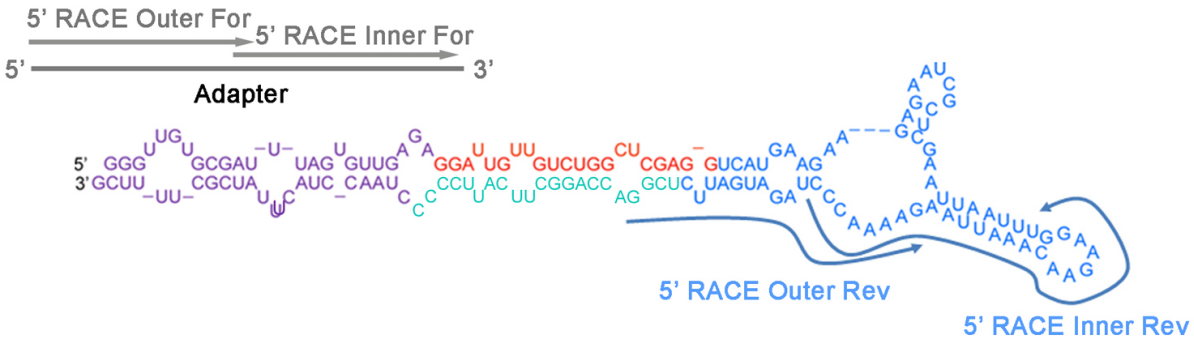
5' RACE Outer For
5' RACE Inner For
5'
3'
Adapter
5' RACE Outer Rev
5' RACE Inner Rev

c

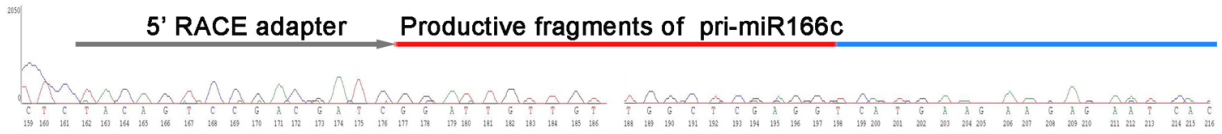
5' RACE adapter
Productive fragments of pri-miR166c

d

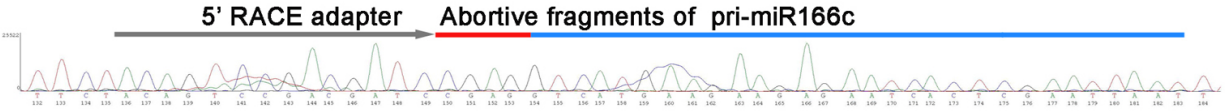
5' RACE adapter
Abortive fragments of pri-miR166c

e

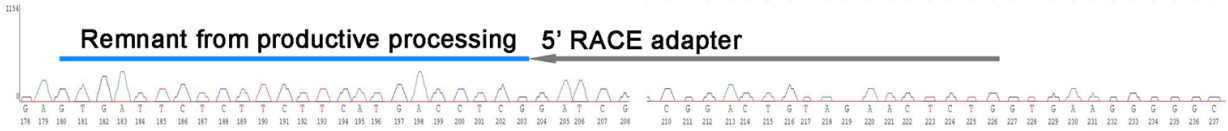
Remnant from productive processing
5' RACE adapter

Supplementary Figure 3. Experimental confirmation of *in vitro* and *in vivo* processed products of pri-miR166c. (a) *In vitro* DCL1 reconstitution assay with pri-miR166c. The reaction products from the assay were spiked with RNA markers before fractionation on a 15% denaturing gel. The positions of intact substrates, cleavage products, and RNA markers are shown. CK, negative control check. (b) Strategic illustration for 5′ RACE assays of intermediate processed products derived from pri-miR166c in planta. Sequences for adapters and primers are provided in Supplementary table 1. (c-e) Sample sequences for a productive-processing (c) and an abortive-processing (d) fragment from pri-miR166c as well as a processing remnant from pre-miR166c (e). 5′-RLM-RACE products were cloned into pENTR vector and plasmids prepared from individual colonies were sequenced with M13 Forward (c and d) and M13 Reverse primers (e).

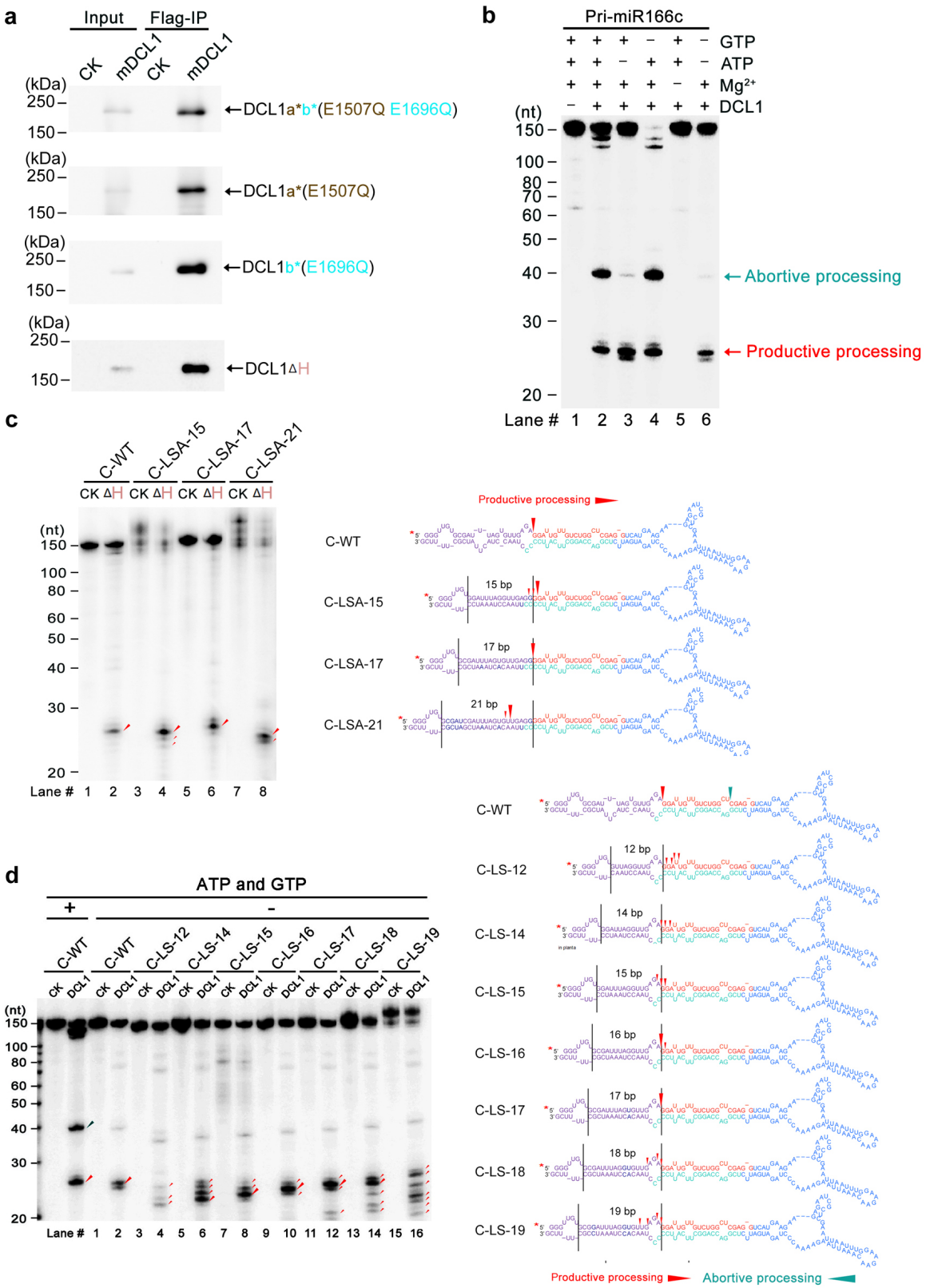
a
Input
Flag-IP
CK
mDCL1
CK
mDCL1
(kDa)
250
150
←DCL1a*b*(E1507Q E1696Q)
←DCL1a*(E1507Q)
←DCL1b*(E1696Q)
←DCL1ΔH
b
Pri-miR166c
GTP
ATP
Mg2+
DCL1
(nt)
150
100
80
70
60
50
40
30
20
← Abortive processing
← Productive processing
Lane # 1 2 3 4 5 6
c
C-WT
C-LSA-15
C-LSA-17
C-LSA-21
CK ΔH
Lane # 1 2 3 4 5 6 7 8
Productive processing
15 bp
17 bp
21 bp
d
ATP and GTP
+
-
C-WT
C-LS-12
C-LS-14
C-LS-15
C-LS-16
C-LS-17
C-LS-18
C-LS-19
ck
DCL1
Lane # 1 2 3 4 5 6 7 8 9 10 11 12 13 14 15 16
12 bp
14 bp
15 bp
16 bp
17 bp
18 bp
19 bp
Productive processing
Abortive processing

Supplementary Figure 4. Helicase domain of DCL1 is essential for abortive processing of pri-miR166c. (a) Western blot analysis of purified DCL1 mutants (mDCL1) using a polyclonal anti-Myc antibody. Immunoprecipitates containing DCL1 (a* or b*, or a* b*) or DCL1 (ΔH) were prepared as described as in Figure 2b. (b) In vitro DCL1 reconstitution assays with 5′ end ^{32}P-labeled pri-miR166c transcripts with or without ATP and GTP. (c) *In vitro* DCL1 (ΔH) reconstitution assays of pri-miR166c mutants with fully complementary lower stems. Schematic illustration of the cleavage products by DCL1 (ΔH) is shown on right. (d) *In vitro* DCL1 reconstitution assays with pri-miR166c mutants with varying distances between internal loops and the reference sites without ATP and GTP. Schematic illustration of the cleavage products is similar to Figure 5d. For panels (b-d), immunoprecipitation, cleavage assays and processing of RNA products were performed as described in Figure 2b. The positions of intact substrates, cleavage products, and RNA markers are marked. Black lines mark the locations of reference sites and internal loops. Red asterisks on the transcripts indicate ^{32}P-labelling positions. Large and small red arrows show the predominant and minor cleavage sites while turquoise arrows indicate abortive processing sites. Note: predominant cleavages at the edges of internal loops in C-LS-18 and C-LS-19 in Panel (d) were less obvious compared to those in Figure 5a.

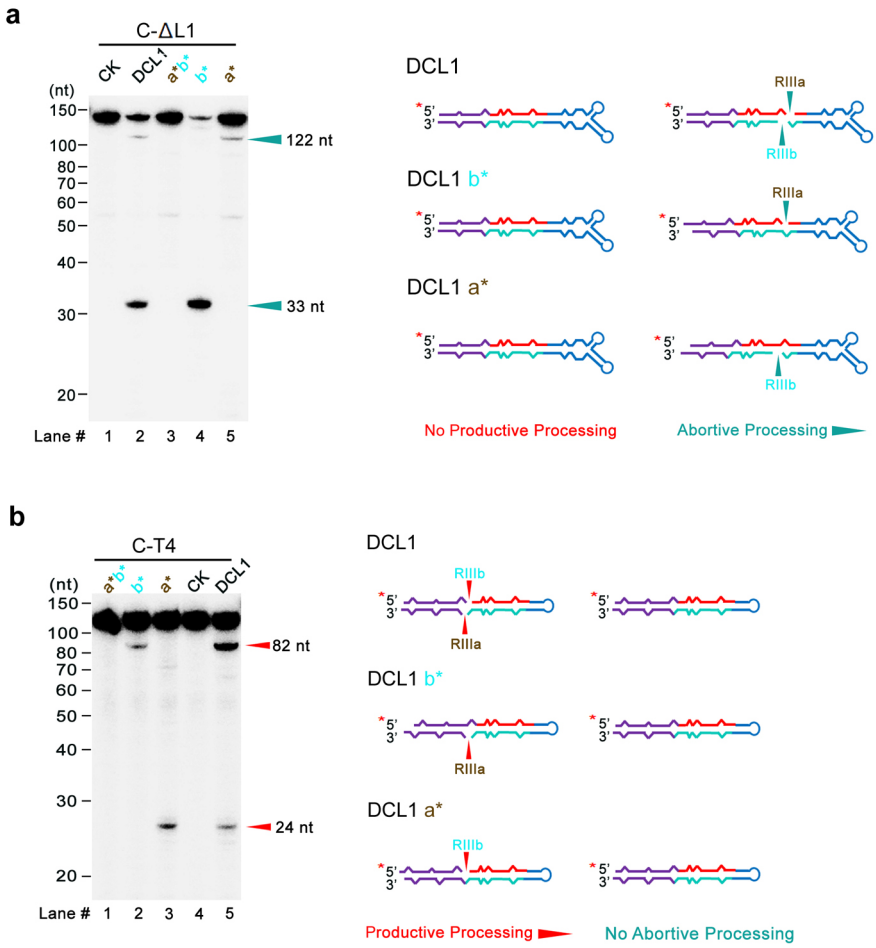

Supplementary Figure 5. Identification of processing direction of pri-miR166c mutants using semi-active DCL1 protein. (a) *In vitro* DCL1 reconstitution assays with the 5′ end labeled pri-miR166c (ΔL1) transcripts. Schematic illustration of the cleavage products by DCL1 or DCL1 mutants is shown on right. Red asterisk on transcripts indicate the ^{32}P-labelling positions. Turquoise arrows indicate the abortive processing sites. (b) *In vitro* DCL1 reconstitution assays with the 5′ end labeled pri-miR166c (C-T4) transcripts. Immunoprecipitation, cleavage assays and processing of RNA products were performed as in Figure 2b. The positions of intact substrates, cleavage products, and RNA markers are shown. Schematic illustration of the cleavage products by DCL1 or DCL1 mutants is shown on right. Red asterisks on the transcripts indicate ^{32}P-labelling positions. Red arrows show the productive processing sites.

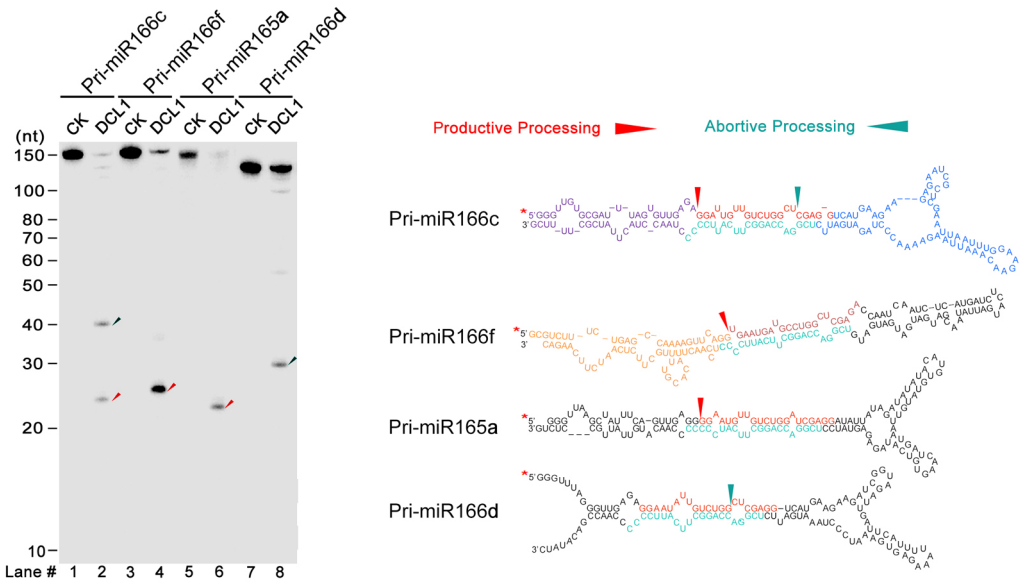

Supplementary Figure 6. *In vitro* DCL1 reconstitution assays with the 5′ end labeled transcripts of pri-miR165a and -miR166d. Immunoprecipitation, cleavage assays, and processing of RNA products were described as Figure 2b. The positions of intact substrates, cleavage products, and RNA markers are shown. Schematic illustration of the cleavage products by DCL1 is shown on right. Red asterisks on the transcripts indicate ^{32}P-labelling positions. Red arrows show the expected productive cleavage sites while turquoise arrows indicate abortive processing sites.

a

Pri-miR162a

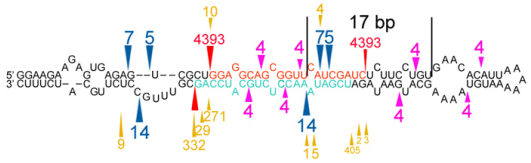

b

Pri-miR171a

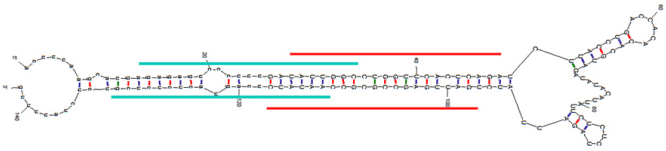

Pri-miR393a

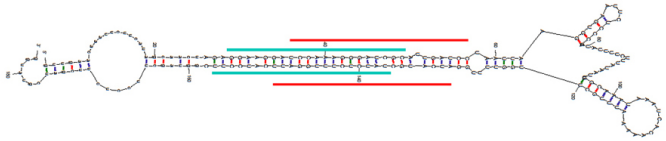

Pri-miR394b

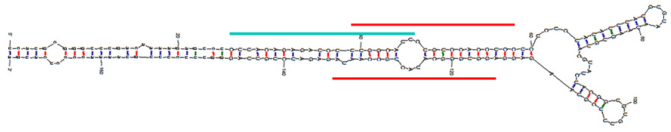

Pri-miR396a

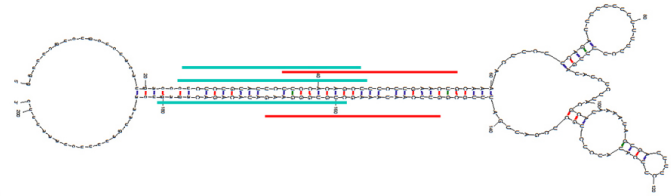

Pri-miR859

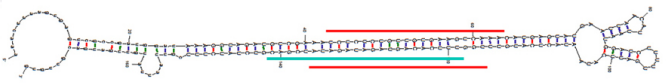

c

Osa Pri-miR162a

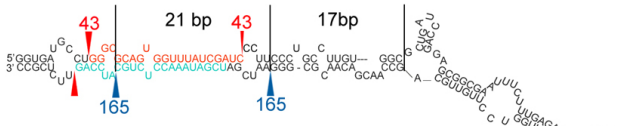

Osa Pri-miR166c

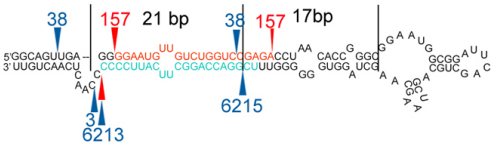

Osa Pri-miR1427

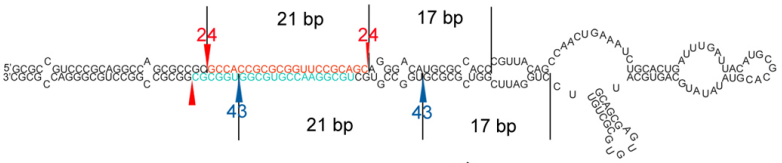

Osa Pri-miR1879

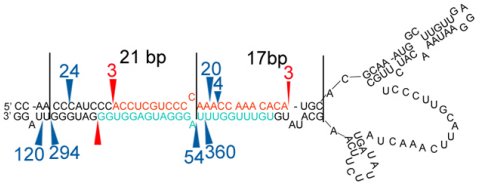

Supplementary Figure 7. Bi-directional processing of pri-miRNAs extends beyond pri-miR166 family and beyond Arabidopsis. (a) An example of bi-directional processing of pri-miRNAs with large internal loops in Arabidopsis. (b) Secondary structures of pri-miRNAs with extended sequences in 5′ and 3′ arms predicted from Mfold program. Red and turquoise lines show locations of productive and abortive processing. (c) Evidence of bi-directional processing of pri-miRNAs with branched terminal loops in rice. For Panel (a and c) miRNA and miRNA* are marked in turquoise and red, respectively. Red arrows (▲) and numbers show productive processing sites and counts of miRNA* reads. Blue arrows (▲) and numbers show positions and counts of sRNAs resulting from apparent abortive processing events. Pink arrows (▲) and numbers show positions and counts of sRNAs resulting from yet unappreciated processing events. Gold arrows (▲) and numbers show 5′ positions and counts of degradome reads, pooled from eight distinct libraries[22,41-43]. The distance from abortive processing sites to internal / terminal loops or between processing sites is shown between two black lines. Note: reads of miRNAs are not shown because they are not unique for individual pri-miRNA paralogs. Minor forms of miRNA/*s that are progressively away from predominant miRNA/* loci are not shown and can be referred in Supplemental Tables 2 and 3.

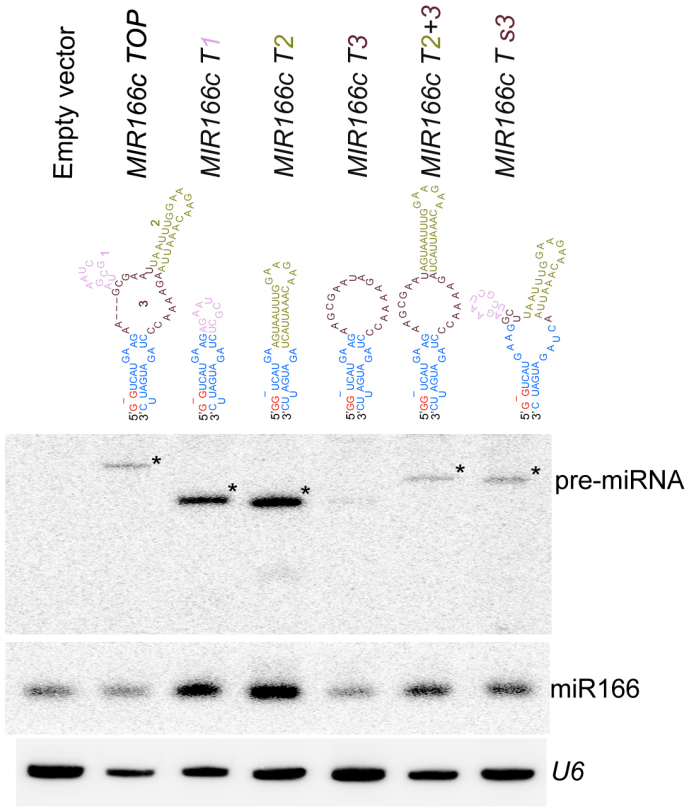

Supplementary Figure 8. RNA blot analyses of pre-miR166 and miR166 in *N. bentha* transiently expressing *35S-MIR166c* mutants. RNA blot was probed using ^{32}P-labelled oligo probes complementary to the indicated miRNA or pre-miRNA. *U6* serves as a loading control. The black asterisks indicate pre-miRNAs.

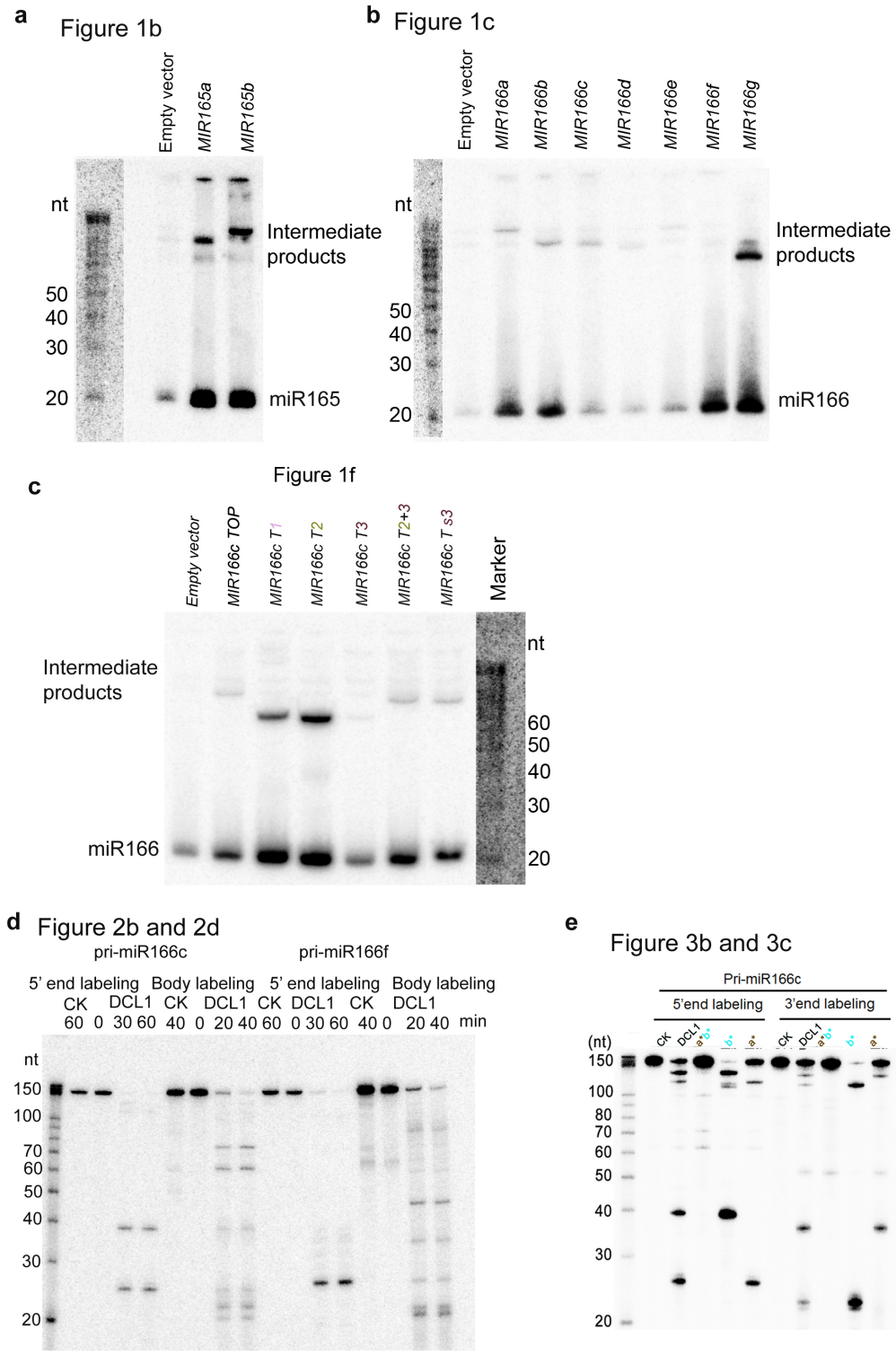

Supplementary Figure 9. Original images of key blots and autoradiographs used in this study. (a) Refer to Fig. 1b. (b) Refer to Fig.1c. (c) Refer to fig. 1f. (d) Refer to Fig. 2b,d. (e) Refer to Fig.3b,c.

SUPPLEMENTARY TABLE LIST

Supplementary Table 1. Primers used in this study.

Supplementary Table 2. Reads of sRNAs generated from bi-directional processing of selected Arabidopsis pri-miRNAs.

Supplementary Table 3. Reads of sRNAs generated from bi-directional processing of selected pri-miRNAs in rice.